JACS
JOURNAL OF THE AMERICAN CHEMICAL SOCIETY
pubs.acs.org/JACS
Article

O-Heterocycle Synthesis via Intramolecular C−H Alkoxylation Catalyzed by Iron Acetylacetonate

Yuyang Dong, Alexandra T. Wrobel, Gerard J. Porter, Jessica J. Kim, Jake Z. Essman, Shao-Liang Zheng, and Theodore A. Betley*

Cite This: J. Am. Chem. Soc. 2021, 143, 7480−7489
Read Online
ACCESS | Metrics & More | Article Recommendations | Supporting Information

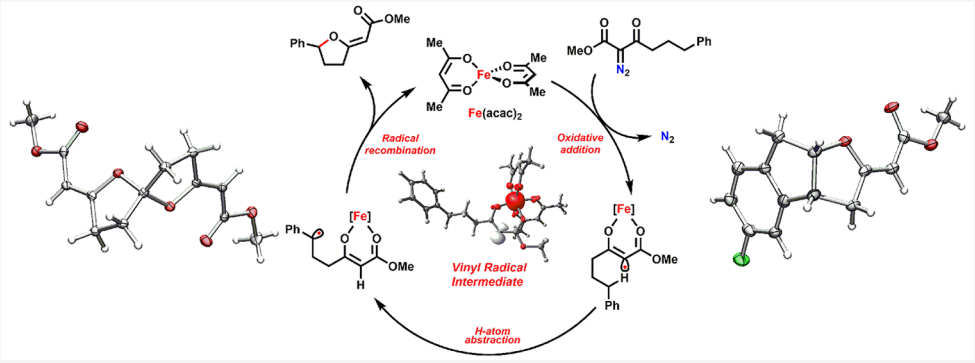

ABSTRACT: Intramolecular alkoxylation of C−H bonds can rapidly introduce structural and functional group complexities into seemingly simple or inert precursors. The transformation is particularly important due to the ubiquitous presence of tetrahydrofuran (THF) motifs as fundamental building blocks in a wide range of pharmaceuticals, agrochemicals, and natural products. Despite the various synthetic methodologies known for generating functionalized THFs, most show limited functional group tolerance and lack demonstration for the preparation of spiro or fused bi- and tricyclic ether units prevalent in molecules for pharmacological purposes. Herein we report an intramolecular C−H alkoxylation to furnish oxacycles from easily prepared α-diazo-β-ketoesters using commercially available iron acetylacetonate ($Fe(acac)_2$) as a catalyst. The reaction is proposed to proceed through the formation of a vinylic carboradical arising from N_2 extrusion, which mediates a proximal H−atom abstraction followed by a rapid C−O bond forming radical recombination step. The radical mechanism is probed using an isotopic labeling study (vinyl C−D incorporation), ring opening of a radical clock substrate, and Hammett analysis and is further corroborated by density functional theory (DFT) calculations. Heightened reactivity is observed for electron-rich C−H bonds (tertiary, ethereal), while greater catalyst loadings or elevated reaction temperatures are required to fully convert substrates with benzylic, secondary, and primary C−H bonds. The transformation is highly functional group tolerant and operates under mild reaction conditions to provide rapid access to complex structures such as spiro and fused bi-/tricyclic O-heterocycles from readily available precursors.

1. INTRODUCTION

Tetrahydrofuran (THF) structures, among other oxygen-containing heterocycles, are fundamental structural units often encountered in a wide range of pharmaceuticals, agrochemicals, and natural products.[1−8] Indeed, THF-containing drugs such as darunavir are among the top 200 pharmaceuticals by retail sales in 2019,[9] while thousands of marine products such as macrolides with oxacyclic building blocks are isolated each year, providing candidates for future pharmacological developments.[1] The high cation affinity and potency as hydrogen bond acceptors make the cyclic ethers potential candidates to alter membrane ion permeability to function as antibiotics[1] and to replace peptidic features of protease inhibitors for antiviral HIV treatments, respectively.[5] Although a variety of methodologies have been developed to synthesize functionalized THF motifs,[7,10−16] most show limited functional group tolerance and are ill-suited for preparing spiro or fused bi- and tricyclic structural units prevalent in most of the applications listed above.[1,6] Recently, Trost and co-workers published their Pd-catalyzed method to drive a [3 + 2] cycloaddition employing an oxyallyl cation to prepare a range of bi- and tricyclic fused structures (Figure 1a).[16] However, the catalysis is limited by the necessity of a conjugated diene, while it is also less effective toward the

Received: February 22, 2021
Published: May 5, 2021

https://doi.org/10.1021/jacs.1c02074
J. Am. Chem. Soc. 2021, 143, 7480−7489

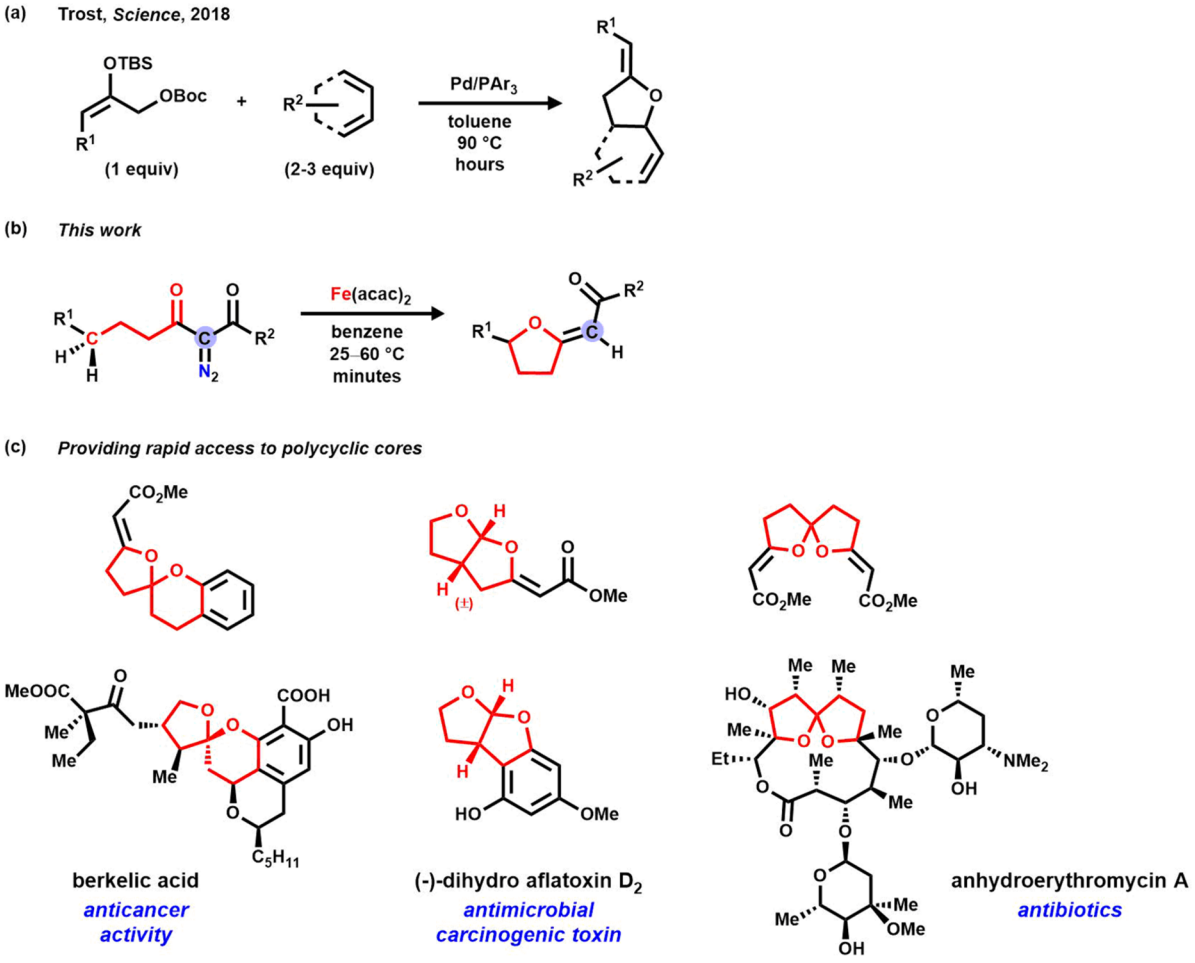

Figure 1. Synthesis of substituted tetrahydrofuran skeletons: (a) Pd-catalyzed [2 + 3] cycloaddition reported by Trost;[16] (b) Fe-catalyzed C−H bond alkoxylation in this report to generate polycyclic, substituted tetrahydrofuran cores; (c) natural products featuring polycyclic tetrahydrofuran cores used as antimicrobial, anticancer, and antibiotic agents.

formation of spiro constructs. Direct C−H functionalization provides an alternative route to rapidly introduce different structural and functional group complexities into seemingly simple or inert precursors. Thus, we were interested in the direct alkoxylation of ubiquitous C−H bonds to synthesize cyclic ethers.

Transition metal-mediated C−H bond functionalization has greatly expanded our capabilities for the elaboration of simple organic feedstocks. Traditional methods feature transition metal stabilization of reactive intermediates which are, in turn, inserted into C−H bonds.[17−21] For example, Rh_2-mediated carbene insertion can be performed with exquisite regio- and enantioselectivity wherein an electrophilic carbene unit inserts into substrate E−H bonds in a concerted fashion.[20−23] For transition metal-stabilized reactive intermediates featuring open-shell configurations, the multiply bonded functionality can exhibit radicaloid character and alter the functionalization trajectory. Indeed, hydroxylation in cytochrome P450[24] occurs via H−atom abstraction (HAA) by the ferryl unit followed by radical recombination (RR) between the Fe^{IV} hydroxyl and carboradical generated. The oxo-unit participation in the electroactive orbitals allows the radical chemistry to proceed. New abiological methodologies have emerged following this precedent, wherein carbene and nitrene C−H insertion catalyzed by a metal porphyrin or analogues[25−34] and C−H amination via dipyrrin-supported metal nitrenoids[35−48] are likewise mediated by metalloradicals. In this report, we describe the generation of a highly reactive vinylic radical via dinitrogen extrusion from α-diazo-β-ketoester substrates by a simple iron catalyst. The generated vinyl radical serves to homolytically cleave intramolecular C−H bonds followed by radical recombination with an open-shell iron alkoxide to furnish tetrahydrofuran skeletons (Figure 1b,c).

2. RESULTS AND DISCUSSION

2.1. O-Heterocycle Formation by Fe Catalyst. The reaction of α-diazo-β-ketoesters with late transition metals typically furnishes the carbocyclic product following carbene generation.[17,21,22,49,50] To study the effect of metalloradical generation on the reactivity, we examined the reaction of methyl 2-diazo-3-oxo-6-phenylhexanoate (**1**) with various iron salts or complexes (Table S1) with accessible Fe^{III}/Fe^{II} redox couples for radical generation.[51] We observed vigorous effervescence at room temperature using a catalytic amount (30 mol %) of inexpensive, commercially available $Fe(acac)_2$ with **1**, upon which the solution changed from dark to bright orange. In contrast to the carbocyclic product observed with Rh_2 catalysis,[49,52] the ^{1}H NMR spectrum of the reaction mixture showed full conversion of **1** into methyl (*Z*)-2-(5-phenyldihydro-2(3*H*)-furanylidene)acetate (**2**; Figures 1b and 2a) after 3 h. The product **2** was further confirmed by multinuclear NMR spectroscopy and single-crystal X-ray

https://doi.org/10.1021/jacs.1c02074
J. Am. Chem. Soc. 2021, 143, 7480−7489

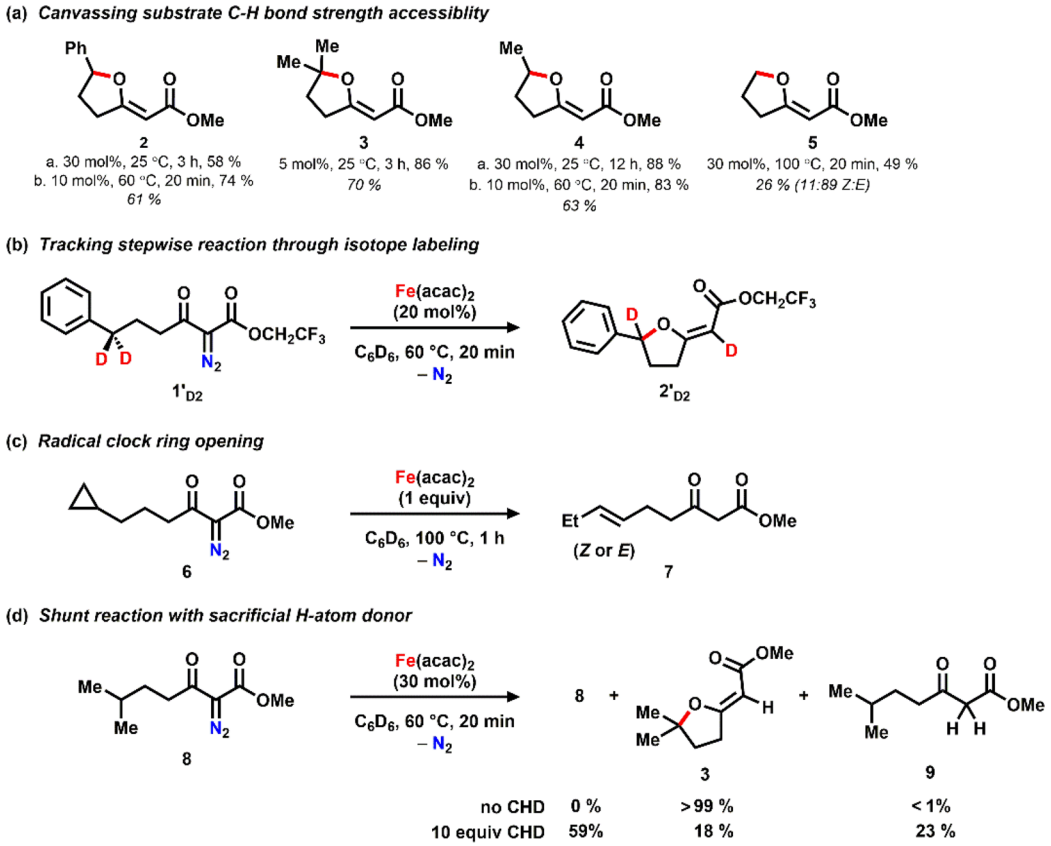

Figure 2. Mechanistic probes for the catalytic synthesis of substituted tetrahydrofurans: (a) establishing C−H bond strength accessible by vinylic radical intermediate; (b) tracing the H−atom abstraction pathway via substrate isotopic labeling; (c) observing radical ring opening of the cyclopropyl substituent; and (d) short-circuiting C−O bond formation via radical recombination with sacrificial 1,4-cyclohexadiene (CHD). Different reaction conditions for full substrate conversion and corresponding NMR yields are given with alphabetical labels. Isolated product yields using the higher-yielding conditions are given in italics at the end.

crystallography (see p 239 in the Supporting Information). The *E* isomer was undetected in the ^{1}H NMR spectrum of the product mixture, suggesting a high level of stereoselectivity for the reaction. We observed exclusive formation of the substituted 2-alkylidene-dihydrofuran generated via cleavage of the benzylic C−H bond along with the formation of new benzylic C−O and vinyl C−H bonds. Similar C−O coupled products both inter- and intramolecularly were previously observed in precious metal-mediated carbene C−H insertion catalysis.[53−56] We hypothesized that the exclusive formation of the *Z* isomer was due to chelation of both the ketone and ester carbonyl O atoms to the Fe center, dictating the olefin conformation. A similar *β*-ketoester substrate binding mode was invoked in six-coordinate iron complexes in enantioselective fluorination and hydroxylation reactions,[57] while a chelated carboradical has recently been proposed to account for the *Z* selectivity in cobalt-mediated olefin isomerization catalysis.[58] Furthermore, theoretical calculations[59] comparing different substrate binding modes revealed the lowest barrier toward N_2 expulsion with the proposed coordination geometry (see p 463 in the Supporting Information). To test for the possibility that the transformation is carried out by colloidal iron formed *in situ*, the catalysis was monitored by dynamic light scattering spectroscopy (DLS), and no absorption was observed for particle sizes between 0.1 and 10^4 nm.

To explore the range of C−H bond strengths activatable for this cyclization reaction, we prepared a series of substrates featuring different types of C−H bonds (**2**−**5**, Figure 2a). Akin to the dirhodium carbene catalysis,[21−23,49,50,52] tertiary C−H bonds (**3**) are the most reactive, achieving complete conversion over 3 h at 25 °C with 5 mol % of Fe(acac)$_2$ (70%). Despite the longer reaction time (3−12 h) and higher catalyst loadings (30 mol %) required to fully consume benzylic (**2**) and secondary substrates (**4**) at room temperature, rapid reactions (20 min) were observed in both cases at 60 °C with 10 mol % Fe(acac)$_2$, leading to overall comparable results. Substrates featuring primary C−H bonds (**5**), on the other hand, showed minimal conversion at 25 °C. An increased reaction temperature (100 °C) with increased catalyst loading (30 mol %), however, enabled the reaction to proceed. The catalysis is stereospecific in every case. as indicated by crude NMR spectra of the product mixture (see the Supporting Information), while olefin isomerization often takes place during product purification due to the relative thermodynamic instability of the *Z* isomer in polar environments.[61] Despite the preference for tertiary C−H bonds observed here being similar to the dirhodium-catalyzed carbene insertion chemoselectivity,[22,49,50,52] the origins of the selectivity are distinctly different. The dirhodium carbene insertion is proposed to arise from the highly electrophilic dirhodium carbene intermediates, activating electron-rich C−H bonds in a concerted fashion.[22,49,50,52] Although a similar concerted reaction trajectory is unlikely in the present alkoxylation reaction, the ease with which tertiary C−H bonds are broken suggests partial oxidation of the C−H bond during the activation step.

https://doi.org/10.1021/jacs.1c02074
J. Am. Chem. Soc. 2021, 143, 7480−7489

2.2. Probing the Alkoxylation Mechanism. As multiple bonds are cleaved (C−N_2, C−H) and formed (vinyl C−H, C−O) during the cyclization of **1**, we sought to identify the reactive intermediate that initiates the transformation. To probe the reaction initiation, isotopically labeled $\mathbf{1'}_{D2}$ was prepared and subjected to the standard catalytic conditions to trace the destination of the benzylic D atom initially abstracted (Figure 2b). The corresponding product $\mathbf{2'}_{D2}$ confirmed the incorporation of deuterium atoms in both the vinylic and benzylic positions (Figure S3), suggesting that the vinyl carbon is indeed responsible for the initial C−H cleavage event. Furthermore, incorporation of a cyclopropyl radical clock into substrate **6** (Figure 2c) and subjecting it to catalytic conditions led to ring opening of the cyclopropyl unit (Figure S7).[62] As a result, we propose two potential mechanisms for the initial C−H activation while accounting for the heightened reactivity toward electron-rich tertiary C−H bonds: (1) a radical type H−atom abstraction with predominantly electron transfer (ET) character during the transition state[63−65] or (2) C−H bond heterolysis via a hydride abstraction pathway.[66] Following the proposed chelation binding mode of the substrate to $Fe(acac)_2$,[57] a radical mechanism (mechanism 1) is initiated by single-electron transfer from iron to the substrate carbonyl to arrive at an open-shell, $Fe(acac)_3$-like intermediate. In the alternative pathway (mechanism 2), the catalyst remains in a ferrous state and merely stabilizes the vinyl carbocation via substrate chelation. The *in situ* generated vinyl carbocation then undergoes a hydride abstraction mechanism (see Figure S1 for the proposed hydride transfer pathway). Since the transition metal center is not involved in any redox event in a hydride transfer mechanism, we examined the catalytic efficacy of $Zn(acac)_2$ to test this proposal where Zn is a redox-inactive, similarly sized[71] Lewis acid surrogate for $Fe(acac)_2$ for the transformation of **1** to **2**. We observed no cyclized product after prolonged (12 h) heating (100 °C) with stoichiometric $Zn(acac)_2$ (Table S1), arguing against this proposed hydride transfer mechanism. An examination of the kinetic profiles for a range of para-substituted benzylic substrates permitted a Hammett analysis (**16**−**19**), which shows a small, negative slope (ρ = −0.30, Figure 3) in contrast to the large correlation expected (i.e., $\rho \approx -2$ for benzylic S_N1 substitution)[60,72,73] for the formation of a benzylic carbocation in the hydride abstraction pathway. To shed light on the reactive intermediate, we performed structural optimization *in silico*, and unpaired electron distribution of the proposed active species were derived using density functional theoretical calculations.[59] The resulting spin-density plot (Figure 4) indeed showed a significant amount of spin delocalized onto the vinyl carbon rather than fully residing on the Fe center, further supporting the single-electron oxidation of iron following dinitrogen extrusion, priming the vinyl radical for a subsequent radical-mediated H−atom abstraction.

To further elucidate the mechanism enabling this transformation, the concentration profiles of substrate, product, and identifiable Fe-containing species were monitored using ^{1}H NMR spectroscopy over the course of the reaction. The catalytic formation of **3** in C_6D_6 was examined at room temperature with 5 mol % of $Fe(acac)_2$ (Figure S6). Two Fe-containing species were identified in the paramagnetic region of the ^{1}H NMR spectrum during the reaction: $Fe(acac)_2$ and a ferric species that has features similar to those of $Fe(acac)_3$. More than 90% of substrate conversion to **3** took place within the first 30 min, with the conversion of $Fe(acac)_2$ into a ferric

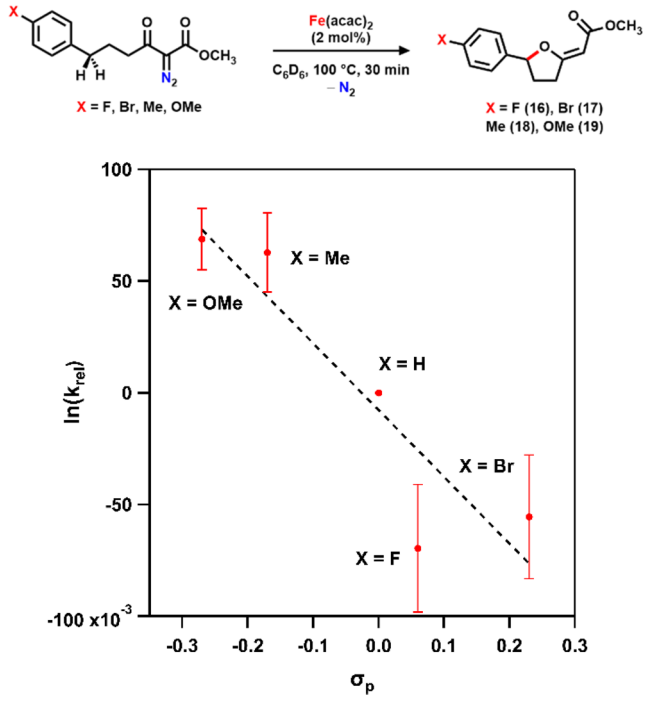

Figure 3. Hammett analysis using an excess amount of substrate to generate products **16**−**19** in competition with an equimolar amount of proteo substrate **2** (ρ = −0.30).[60]

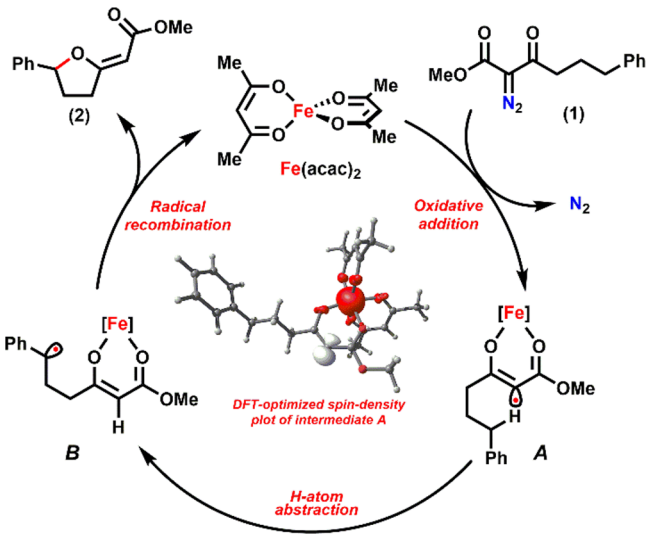

Figure 4. Proposed catalytic mechanism for the synthesis of substituted tetrahydrofurans.

compound as detected by ^{1}H NMR spectroscopy. We note that a significant amount of product **3** (~10%) was already found at the first time point taken (1 s), consistent with a high reaction rate at the beginning of the transformation. The turnover frequency dropped significantly upon lowering the amount of $Fe(acac)_2$ with almost no further conversion (<5%) after its disappearance, suggesting that $Fe(acac)_2$ was directly involved in the cyclization. Unfortunately, due to facile catalyst deactivation, a detailed rate law cannot be derived.

We propose the ferric species results from (1) the disproportionation of $Fe(acac)_2$ with concomitant production of a reduced Fe species or (2) the coordination of enolates (**9**, Figure 2d) generated from reduced α-diazo-β-ketoesters via

https://doi.org/10.1021/jacs.1c02074
J. Am. Chem. Soc. 2021, 143, 7480−7489

HAT from adventitious H−atom sources. The lack of observable colloidal particles by DLS spectroscopy argues against the generation of insoluble reduced iron species. To provide evidence on the second proposed pathway, the transformation from **8** to **3** was carried out with 30 mol % of $Fe(acac)_2$ in both the absence and presence of 1,4-cyclohexadiene (CHD) (Figure 2d). Vigorous effervescence was observed in both reactions, and the ^1H NMR spectra taken after the bubbling ceased showed partial and full conversion of $Fe(acac)_2$ into the ferric species in the absence and presence of CHD, respectively. Following an acidic workup, near-quantitative conversion of **8** to **3** was observed in the absence of CHD, while a significant quantity of **9** (23%) diminished the amount of product **3** (18%), and the remaining starting material **8** (59%) was found with the exogenous H−atom source added (Figure S4). The result supports our second hypothesis that catalyst deactivation is caused by HAT from adventitious H−atom sources.

On the basis of the foregoing results, we propose the following catalytic cycle shown in Figure 4. Substrate binding to $Fe(acac)_2$ occurs through the ketoester functionalities. Electron transfer from the Fe center reduces the keto functionality and triggers dinitrogen loss, resulting in a stable, high-spin $S = 5/2$ Fe(III) center and a vinyl carboradical. The vinyl carboradical undergoes 1,5-HAT with predominant ET character during the transition state. The alkyl carboradical generated *in situ* from the HAT step combines with the keto oxygen bound to iron to furnish the (*Z*)-2-alkylidene dihydrofuran. Theoretical calculations[59] simulating the reaction of substrates with benzylic (**2**), tertiary (**3**), and secondary C−H bonds (**4**) revealed a rate-determining N_2 loss step (RDS) with an activation barrier of ca. 21.4 kcal/mol (Figure 6), consistent with the reaction taking place at room temperature. The subsequent HAA step is computed to be the most favorable for tertiary C−H activation (2.9 kcal/mol for **3** vs 6.0 and 6.8 kcal/mol for **2** and **4**, respectively), followed by barrierless radical recombination processes[35] to yield the final (*Z*)-2-alkylidene dihydrofuran product. Despite the similar calculated rate-determining N_2 loss barriers for **2**−**4** (Figure 6), we propose that the differences in reactivities observed experimentally were due to the post-RDS catalyst deactivation in competition with the productive HAA barrier. For substrates that are harder to activate, a relatively higher rate for catalyst deactivation is expected, leading to the overall lower reactivity observed, while for substrates with more reactive C−H bonds, the HAA step is more kinetically competitive against the catalyst deactivation, resulting in more rapid catalytic turnovers and lower catalyst loadings.

2.3. Examining the Alkoxylation Selectivity. Remarkably, only products corresponding to activation of the ketone substituents from the α-diazo-β-ketoesters were observed. Substrates (Figure 5a, **10** and **11**) featuring benzylic C−H bonds on the ester group (phenethyl ester) and benzylic or tertiary C−H bonds on the ketone substituents were prepared and examined under standard catalytic conditions. Products resulting from C−O bond formation with the ester carbonyl O atom were undetected in the ^1H NMR spectrum of the product mixture in both cases. Furthermore, cyclization using α-diazo malonate derivatives (**12**) does not proceed at all after heating to 100 °C for 36 h with stoichiometric amounts of $Fe(acac)_2$, whereas a α-diazo-β-diketone substrate (**13**) undergoes the cyclization at room temperature with 30 mol % catalyst loading. We rationalized the reactivity discrepancy

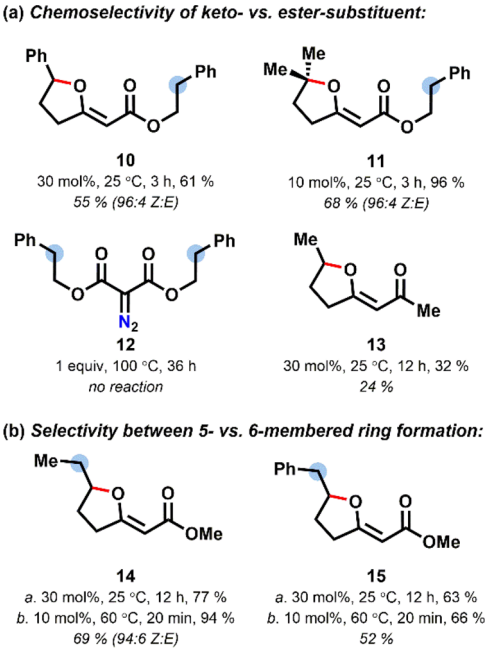

Figure 5. Exploration of C−H bond alkoxylation cyclization reaction examining the chemoselectivity (a) and oxacycle ring-size selectivity (b). Different reaction conditions for full substrate conversion and corresponding NMR yields are given with alphabetical labels. Isolated product yields using the higher-yielding conditions are given in italics at the end.

between cyclization with the ketone versus the ester carbonyl oxygen as the result of differences in their corresponding redox potentials or, alternatively, the electrophilicities between these two functional groups,[74] where the ester carbonyl is more electron rich due to π-donation from the alkoxyl substituent and thus is harder to reduce. Indeed, DFT simulations using the α-diazo malonate derivative **12** showed a much higher barrier for both the N_2 extrusion and HAT steps (Figure 6), corroborating the experimental observation.

Two factors dictate the observed chemoselectivity toward the ring size of the O-heterocycle formed: (1) the relative bond dissociation energy (BDE) differences of the target C−H bonds (enthalpic) and (2) the entropic preference among different ring-forming transition states. To compare these two contributions, **14** was prepared, where secondary C−H bonds were positioned to form either five- or six-membered rings (Figure 5b). ^1H NMR spectroscopy of the product mixture showed exclusive formation of the five-membered-ring-containing product, suggesting an entropic preference toward furan ring formation. To evaluate the strength of this entropic preference, **15** was synthesized in which the weaker, benzylic C−H bond was positioned to form a tetrahydropyran derivative, while the formation of a five-membered cycle necessitates the activation of a stronger, secondary C−H bond. Gratifyingly, a high level of selectivity was similarly observed by ^1H NMR spectroscopy with the sole formation of tetrahydrofuran-containing product **15**, as further verified by single-crystal X-ray diffraction (see p 279 in the Supporting Information). This result suggests that the entropic preference outcompetes enthalpic BDE differences between benzylic and secondary C−H bonds (ca. 8 kcal/mol),[75] further demonstrating the importance of the entropic factor in the product selectivity of this catalytic transformation.

https://doi.org/10.1021/jacs.1c02074
J. Am. Chem. Soc. 2021, 143, 7480−7489

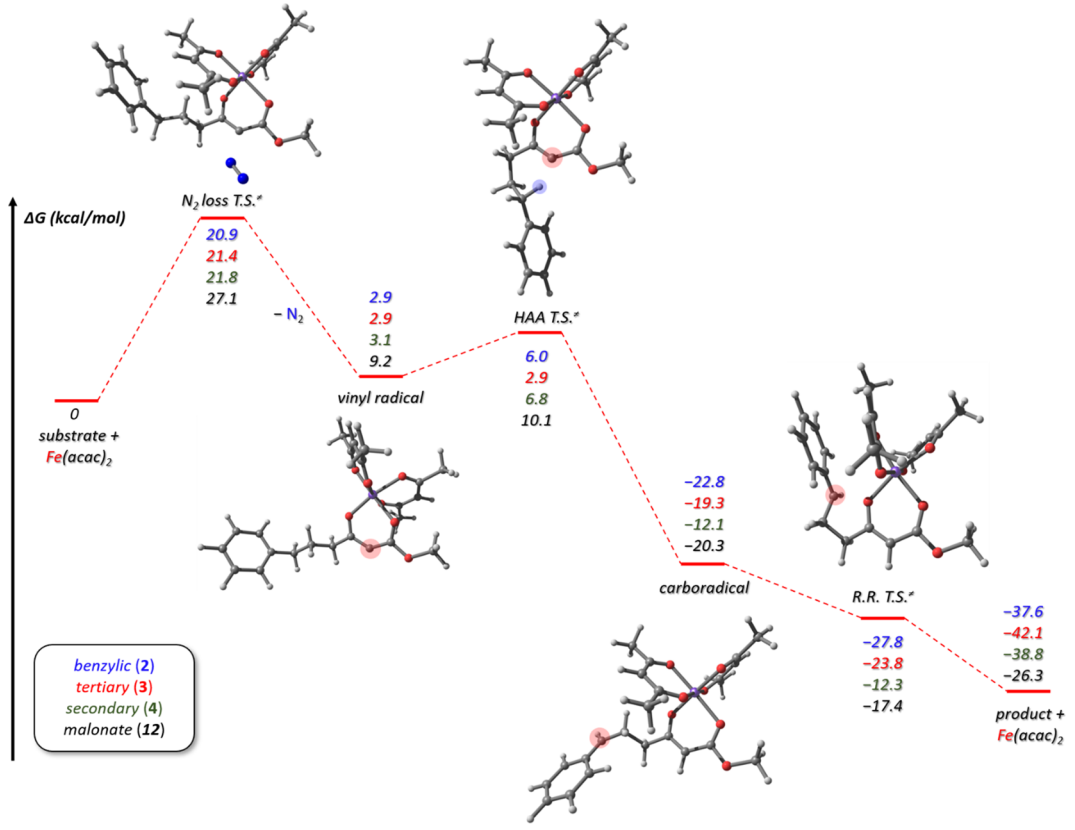

Figure 6. DFT (B3LYP/def2-SVP(C,H),def2-TZVP(Fe,O))[67−70] free energy diagram (in kcal/mol) calculated using the Orca software package[59] for the proposed C−H alkoxylation mechanism for the cyclization of substrates featuring benzylic (**2**) (optimized structures shown), tertiary (**3**), and secondary (**4**) C−H bonds as well as a malonate core structure (**12**) mediated by $Fe(acac)_2$ with energies labeled in blue, red, green, and maroon, respectively.

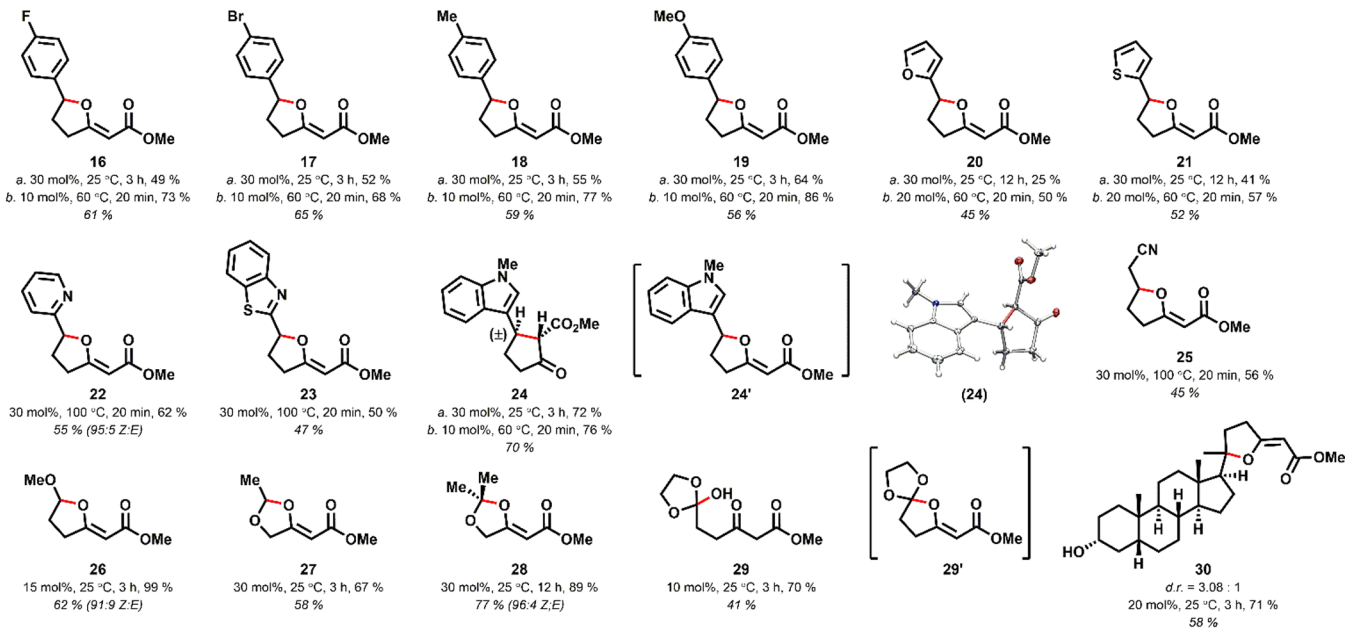

Figure 7. Scope and exploration of C−H bond alkoxylation cyclization reactions examining the substrate functional group tolerance. Different reaction conditions for full substrate conversion and corresponding NMR yields are given with alphabetical labels. Isolated product yields using the higher-yielding conditions are given in italics at the end.

2.4. Expanding the Substrate Scope. The alkoxylation tolerates a wide scope of functional groups (Figure 7, **16**−**30**), while it provides rapid access to a range of complex spiro and fused structures (Figure 8, **32**−**47**). Given the ubiquity of heterocycles in pharmaceuticals, particularly N-containing compounds,[76] the cyclization was probed with a variety of aromatics present, such as furan (**20**), thiophene (**21**), pyridine (**22**), benzothiazine (**23**), and indole (**24**). We note that

https://doi.org/10.1021/jacs.1c02074
J. Am. Chem. Soc. 2021, 143, 7480−7489

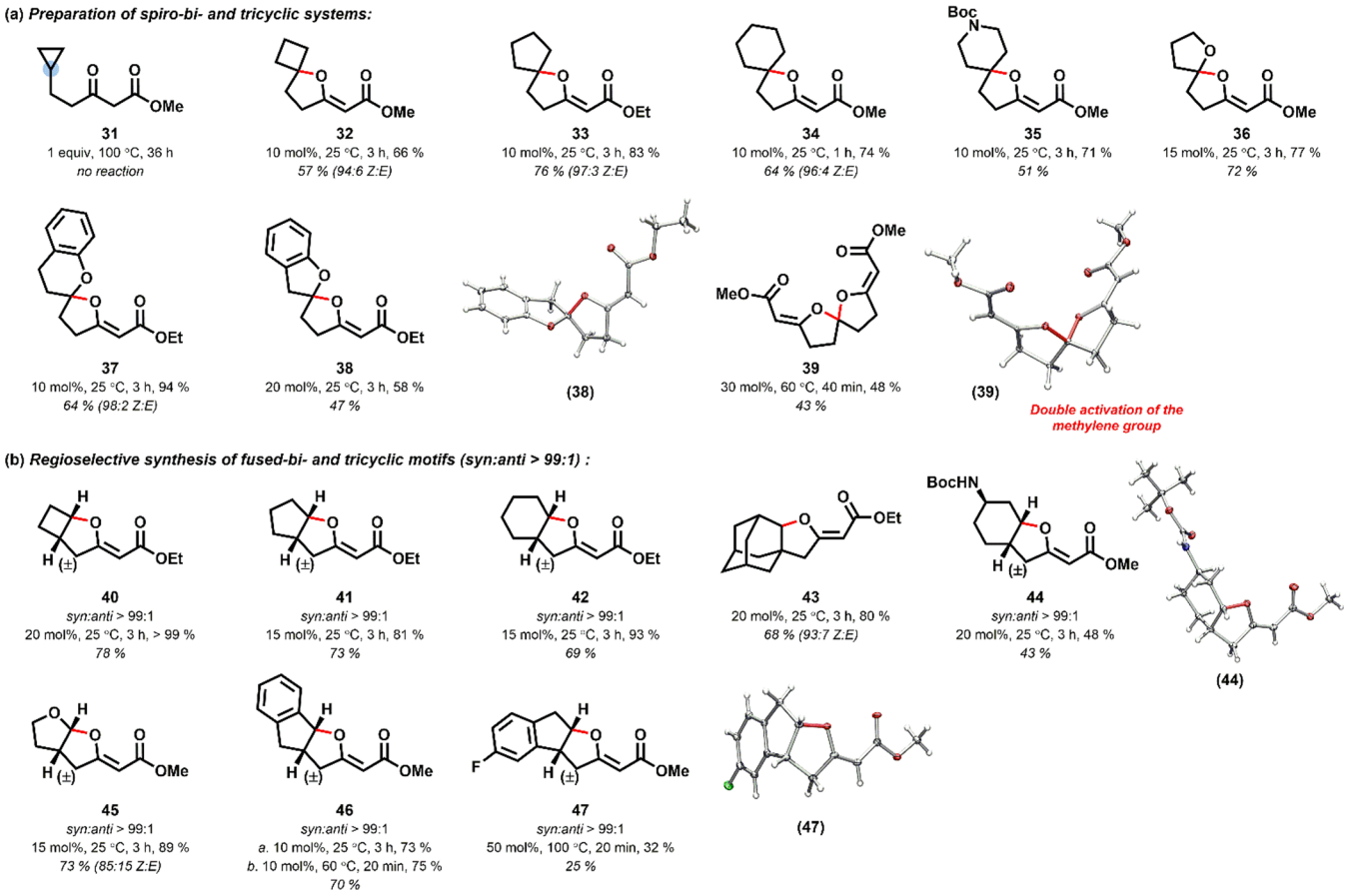

Figure 8. Scope and exploration of C−H bond alkoxylation cyclization reactions examining the efficacy for the generation of spiro bi- and tricyclic systems (a) as well as fused bi- and tricyclic products (b). Different reaction conditions for full substrate conversion and corresponding NMR yields are given with alphabetical labels. Isolated product yields using the higher yielding conditions are given in italics at the end.

increased reaction temperatures (100 °C) were required to drive substrate conversions with electron-deficient heterocycles to completion (**22** and **23**) relative to the electron-rich heterocycles, potentially due to (1) higher C−H bond oxidation potentials due to adjacent electron-withdrawing aryl groups or (2) competing binding of the coordinating N atoms versus substrate ketoester functionalities toward the Fe center. Interestingly, the *N*-methylindole-containing substrate cleanly afforded a product with distinct ^{1}H NMR features after workup, which was further identified by single-crystal X-ray diffraction as the cyclopentanone derivative (**24**) commonly synthesized by rhodium-catalyzed carbene insertion catalysis.[21−23,49,50] Closer inspection of the ^{1}H NMR spectra during catalysis revealed the kinetic formation of the anticipated (*Z*)-2-alkylidene dihydrofuran product (**24′**) that gradually converted into cyclopentanone **24** entirely as its *trans* isomer at 25 °C in $CDCl_3$ (see p 330 in the Supporting Information for the proposed mechanism). Similar transformations have been demonstrated with palladium catalysis via the formation of a π-allyl cation[16] or simple Lewis acid catalysis for 2-alkylidene-4-aryl-4-alkyldihydrofurans with similar stereospecificity.[10] To showcase the ability of functionalization of complex structures and tolerance toward protic functional groups, a substrate featuring a steroid core derived from lithocholic acid (**30**) was prepared and subjected to catalytic conditions at room temperature, affording product **30** in a 3.08:1 mixture of the two diastereomers resulting from alkoxylation of the corresponding tertiary C−H bond. The partial epimerization suggests a slower rate of radical recombination with the carbonyl O atom in comparison to carboradical rotation prior to ring closure.

Due to the electron richness of tertiary and ethereal C−H bonds, spiro bicyclic rings can be readily prepared using substrates featuring four- (**32**), five- (**33**, **36**, **38**, **39**), and six-membered cyclic motifs (**34**, **35**, **37**). The cyclopropyl variant (**31**), however, showed no conversion even under forcing conditions, potentially due to the high *s* character in the target C−H bond.[77] The dioxaspiro building blocks (**36**−**39**) synthesized here are widely present in pharmaceuticals for HIV treatment,[5] in polyether antibiotics, and in a range of natural products.[78] Moreover, to demonstrate the ability of rapidly introducing structural and functional group complexity into simple hydrocarbons, a substrate with multiple diazo units was employed to directly arrive at a biologically relevant spiro bicyclic structure via double activation of the same methylene unit (**39**). Remarkably, fused rings were also readily prepared, providing quick access to a range of bi- and tricyclic structures (**40**−**47**). Notably, excellent stereoselectivity toward the *syn* isomer was observed in every case, with no *anti* isomer detected in the product NMR spectra. Furthermore, high selectivity toward ethereal over secondary C−H bond activation resulted in exclusive formation of the fused bicyclic acetal (**45**), again showcasing the heightened reactivity for alkoxylation of electron-rich C−H bonds.

https://doi.org/10.1021/jacs.1c02074
J. Am. Chem. Soc. 2021, 143, 7480−7489

3. CONCLUSION

The foregoing data describe a methodology for the preparation of structurally complex furan heterocycles employing easily prepared diazo substrates catalyzed by commercially available $Fe(acac)_2$ under mild conditions. Our mechanistic investigation suggested a novel, stereospecific C−H functionalization pathway via the *in situ* formation of a vinyl C-based radical to generate the kinetically stable (*Z*)-2-alkylidene dihydrofurans with high entropic selectivity for five-membered rings and heightened reactivity toward electron-rich C−H bonds. The catalysis is particularly effective in the synthesis of spiro and fused bi- and tricyclic ethers commonly found in agrochemical, pharmaceutical, and natural products.[1−6,9] With the wide functional group tolerance and the generation of enolester motifs,[16] we envision the methodology presented here would provide rapid access to a variety of highly functionalized cyclic, structurally complex ether precursors for elaborated downstream organic synthesis.

■ ASSOCIATED CONTENT

Supporting Information

The Supporting Information is available free of charge at https://pubs.acs.org/doi/10.1021/jacs.1c02074.

General experimental considerations and procedures, multinuclear NMR data, solid state molecular structures, crystallographic details and data, and theoretical calculation methods (PDF)

Accession Codes

CCDC 2003790−2003793 and 2031360−2031365 contain the supplementary crystallographic data for this paper. These data can be obtained free of charge via www.ccdc.cam.ac.uk/data_request/cif, or by emailing data_request@ccdc.cam.ac.uk, or by contacting The Cambridge Crystallographic Data Centre, 12 Union Road, Cambridge CB2 1EZ, UK; fax: +44 1223 336033.

■ AUTHOR INFORMATION

Corresponding Author

Theodore A. Betley − *Department of Chemistry and Chemical Biology, Harvard University, Cambridge, Massachusetts 02138, United States;* orcid.org/0000-0001-5946-9629; Email: betley@chemistry.harvard.edu

Authors

Yuyang Dong − *Department of Chemistry and Chemical Biology, Harvard University, Cambridge, Massachusetts 02138, United States;* orcid.org/0000-0002-4533-4798

Alexandra T. Wrobel − *Department of Chemistry and Chemical Biology, Harvard University, Cambridge, Massachusetts 02138, United States*

Gerard J. Porter − *Department of Chemistry and Chemical Biology, Harvard University, Cambridge, Massachusetts 02138, United States;* orcid.org/0000-0003-3969-548X

Jessica J. Kim − *Department of Chemistry and Chemical Biology, Harvard University, Cambridge, Massachusetts 02138, United States*

Jake Z. Essman − *Department of Chemistry and Chemical Biology, Harvard University, Cambridge, Massachusetts 02138, United States;* orcid.org/0000-0003-2000-2196

Shao-Liang Zheng − *Department of Chemistry and Chemical Biology, Harvard University, Cambridge, Massachusetts 02138, United States;* orcid.org/0000-0002-6432-9943

Complete contact information is available at: https://pubs.acs.org/10.1021/jacs.1c02074

Author Contributions

The manuscript was written through contributions of all authors. All authors have given approval to the final version of the manuscript.

Notes

The authors declare no competing financial interest.

■ ACKNOWLEDGMENTS

This work was generously supported by a grant from the NIH (GM-115815), the Dreyfus Foundation (Teacher-Scholar Award to T.A.B.), and Harvard University. A.T.W. is grateful for a predoctoral fellowship from the NSF.

■ ABBREVIATIONS

CCR2, CC chemokine receptor 2; CCL2, CC chemokine ligand 2; CCR5, CC chemokine receptor 5; TLC, thin-layer chromatography

■ REFERENCES

(1) Lorente, A.; Lamariano-Merketegi, J.; Albericio, F.; Álvarez, M. Tetrahydrofuran-Containing Macrolides: A Fascinating Gift from the Deep Sea. *Chem. Rev.* **2013**, *113*, 4567.

(2) Chorley, D. F.; Furkert, D. P.; Brimble, M. A. Synthesis of the Spiroketal Core of the Pinnatifinoside Family of Natural Products. *Eur. J. Org. Chem.* **2016**, *2016*, 314.

(3) Huang, W.-L.; Raja, A.; Hong, B.-C.; Lee, G.-H. Organocatalytic Enantioselective Michael-Acetalization-Reduction-Nef Reaction for a One-Pot Entry to the Functionalized Aflatoxin System. Total Synthesis of (−)-Dihydroaflatoxin D_2 and (−)- and (+)-Microminutinin. *Org. Lett.* **2017**, *19*, 3494.

(4) Li, Q.; Zhao, K.; Peuronen, A.; Rissanen, K.; Enders, D.; Tang, Y. Enantioselective Total Syntheses of (+)-Hippolachnin A, (+)-Gracilioether A, (−)-Gracilioether E, and (−)-Gracilioether F. *J. Am. Chem. Soc.* **2018**, *140*, 1937.

(5) Ghosh, A. K.; Anderson, D. D. Tetrahydrofuran, tetrahydropyran, triazoles and related heterocyclic derivatives as HIV protease inhibitors. *Future Med. Chem.* **2011**, *3*, 1181.

(6) Fernandes, R. A.; Gorve, D. A.; Pathare, R. S. Emergence of 2,3,5-trisubstituted tetrahydrofuran natural products and their synthesis. *Org. Biomol. Chem.* **2020**, *18*, 7002.

(7) Singh, P. K.; Silakari, O. The Current Status of O-Heterocycles: A Synthetic and Medicinal Overview. *ChemMedChem* **2018**, *13*, 1071.

(8) Taylor, A. P.; Robinson, R. P.; Fobian, Y. M.; Blakemore, D. C.; Jones, L. H.; Fadeyi, O. Modern advances in heterocyclic chemistry in drug discovery. *Org. Biomol. Chem.* **2016**, *14*, 6611.

(9) McGrath, N. A.; Brichacek, M.; Njardarson, J. T. A Graphical Journey of Innovative Organic Architectures That Have Improved Our Lives. *J. Chem. Educ.* **2010**, *87*, 1348.

(10) Fujitani, B.; Hanaya, K.; Sugai, T.; Higashibayashi, S. Stepwise approach for sterically hindered Csp^3-Csp^3 bond formation by dehydrogenative O-alkylation and Lewis acid-catalyzed [1,3]-rearrangement towards the arylalkylcyclopentane skeleton of sesquiterpenes. *Chem. Commun.* **2020**, *56*, 3621.

(11) Shigehisa, H.; Hayashi, M.; Ohkawa, H.; Suzuki, T.; Okayasu, H.; Mukai, M.; Yamazaki, A.; Kawai, R.; Kikuchi, H.; Satoh, Y.; Fukuyama, A.; Hiroya, K. Catalytic Synthesis of Saturated Oxygen Heterocycles by Hydrofunctionalization of Unactivated Olefins: Unprotected and Protected Strategies. *J. Am. Chem. Soc.* **2016**, *138*, 10597.

(12) Goldfogel, M. J.; Roberts, C. C.; Meek, S. J. Intermolecular Hydroamination of 1,3-Dienes Catalyzed by Bis(phosphine)-carbodicarbene-Rhodium Complexes. *J. Am. Chem. Soc.* **2014**, *136*, 6227.

(13) Castarlenas, R.; Vovard, C.; Fischmeister, C.; Dixneuf, P. H. Allenylidene-to-Indenylidene Rearrangement in Arene-Ruthenium Complexes: A Key Step to Highly Active Catalysts for Olefin Metathesis Reactions. *J. Am. Chem. Soc.* **2006**, *128*, 4079.
(14) Masahiko, Y.; Ichiro, H. Reaction of oxiranes with dianion of methyl acetoacetate in the presence of boron trifluoride etherate. *Chem. Lett.* **1985**, *14*, 337.
(15) Zheng, S.-L.; Yu, W.-Y.; Che, C.-M. Ruthenium(II) Porphyrin Catalyzed Formation of (*Z*)-4-Alkyloxycarbonyl-methylidene-1,3-dioxolanes from γ-Alkoxy-α-diazo-β-ketoesters. *Org. Lett.* **2002**, *4*, 889.
(16) Trost, B. M.; Huang, Z.; Murhade, G. M. Catalytic palladium-oxyallyl cycloaddition. *Science* **2018**, *362*, 564.
(17) Bergstrom, B. D.; Nickerson, L. A.; Shaw, J. T.; Souza, L. W. Transition Metal Catalyzed Insertion Reactions with Donor/Donor Carbenes. *Angew. Chem., Int. Ed.* **2021**, *60*, 6864.
(18) Trowbridge, A.; Walton, S. M.; Gaunt, M. J. New Strategies for the Transition-Metal Catalyzed Synthesis of Aliphatic Amines. *Chem. Rev.* **2020**, *120*, 2613.
(19) Kuijpers, P. F.; van der Vlugt, J. I.; Schneider, S.; de Bruin, B. Nitrene Radical Intermediates in Catalytic Synthesis. *Chem. - Eur. J.* **2017**, *23*, 13819.
(20) Gillingham, D.; Fei, N. Catalytic X-H insertion reactions based on carbenoids. *Chem. Soc. Rev.* **2013**, *42*, 4918.
(21) Doyle, M. P.; Duffy, R.; Ratnikov, M.; Zhou, L. Catalytic Carbene Insertion into C-H Bonds. *Chem. Rev.* **2010**, *110*, 704.
(22) Taber, D. F.; Petty, E. H. General route to highly functionalized cyclopentane derivatives by intramolecular C-H insertion. *J. Org. Chem.* **1982**, *47*, 4808.
(23) Werlé, C.; Goddard, R.; Fürstner, A. The First Crystal Structure of a Reactive Dirhodium Carbene Complex and a Versatile Method for the Preparation of Gold Carbenes by Rhodium-to-Gold Transmetalation. *Angew. Chem., Int. Ed.* **2015**, *54*, 15452.
(24) Meunier, B.; de Visser, S. P.; Shaik, S. Mechanism of Oxidation Reactions Catalyzed by Cytochrome P450 Enzymes. *Chem. Rev.* **2004**, *104*, 3947.
(25) Lu, H.; Zhang, X. P. Catalytic C-H functionalization by metalloporphyrins: recent developments and future directions. *Chem. Soc. Rev.* **2011**, *40*, 1899.
(26) Goswami, M.; Lyaskovskyy, V.; Domingos, S. R.; Buma, W. J.; Woutersen, S.; Troeppner, O.; Ivanović-Burmazović, I.; Lu, H.; Cui, X.; Zhang, X. P.; Reijerse, E. J.; DeBeer, S.; van Schooneveld, M. M.; Pfaff, F. F.; Ray, K.; de Bruin, B. Characterization of Porphyrin-Co(III)-Nitrene Radical Species Relevant in Catalytic Nitrene Transfer Reactions. *J. Am. Chem. Soc.* **2015**, *137*, 5468.
(27) Suarez, A. I. O.; Lyaskovskyy, V.; Reek, J. N. H.; van der Vlugt, J. I.; de Bruin, B. Complexes with Nitrogen-Centered Radical Ligands: Classification, Spectroscopic Features, Reactivity, and Catalytic Applications. *Angew. Chem., Int. Ed.* **2013**, *52*, 12510.
(28) Goswami, M.; Geuijen, P.; Reek, J. N. H.; de Bruin, B. Application of [Co(Corrole)]$^-$ Complexes in Ring-Closing C-H Amination of Aliphatic Azides via Nitrene Radical Intermediates. *Eur. J. Inorg. Chem.* **2018**, *2018*, 617.
(29) Griffin, J. R.; Wendell, C. I.; Garwin, J. A.; White, M. C. Catalytic C(sp^3)-H Alkylation via an Iron Carbene Intermediate. *J. Am. Chem. Soc.* **2017**, *139*, 13624.
(30) Clark, J. R.; Feng, K.; Sookezian, A.; White, M. C. Manganese-catalysed benzylic C(sp^3)-H amination for late-stage functionalization. *Nat. Chem.* **2018**, *10*, 583.
(31) Paradine, S. M.; Griffin, J. R.; Zhao, J.; Petronico, A. L.; Miller, S. M.; Christina White, M. A manganese catalyst for highly reactive yet chemoselective intramolecular C(sp^3)-H amination. *Nat. Chem.* **2015**, *7*, 987.
(32) Xiao, W.; Zhou, C.-Y.; Che, C.-M. Ruthenium(IV) porphyrin catalyzed phosphoramidation of aldehydes with phosphoryl azides as a nitrene source. *Chem. Commun.* **2012**, *48*, 5871.
(33) Xiao, W.; Wei, J.; Zhou, C.-Y.; Che, C.-M. [Ru^{IV}(F_{20}-TPP)Cl_2] efficiently catalysed inter- and intra-molecular nitrene insertion into sp^3 C-H bonds of hydrocarbons using phosphoryl azides as nitrene sources. *Chem. Commun.* **2013**, *49*, 4619.
(34) Intrieri, D.; Carminati, D. M.; Gallo, E. Recent advances in C-H bond aminations catalyzed by ruthenium porphyrin complexes. *J. Porphyrins Phthalocyanines* **2016**, *20*, 190.
(35) Iovan, D. A.; Betley, T. A. Characterization of Iron-Imido Species Relevant for N-Group Transfer Chemistry. *J. Am. Chem. Soc.* **2016**, *138*, 1983.
(36) Carsch, K. M.; DiMucci, I. M.; Iovan, D. A.; Li, A.; Zheng, S.-L.; Titus, C. J.; Lee, S. J.; Irwin, K. D.; Nordlund, D.; Lancaster, K. M.; Betley, T. A. Synthesis of a copper-supported triplet nitrene complex pertinent to copper-catalyzed amination. *Science* **2019**, *365*, 1138.
(37) Baek, Y.; Hennessy, E. T.; Betley, T. A. Direct Manipulation of Metal Imido Geometry: Key Principles to Enhance C-H Amination Efficacy. *J. Am. Chem. Soc.* **2019**, *141*, 16944.
(38) Dong, Y.; Clarke, R. M.; Porter, G. J.; Betley, T. A. Efficient C-H Amination Catalysis Using Nickel-Dipyrrin Complexes. *J. Am. Chem. Soc.* **2020**, *142*, 10996.
(39) Dong, Y.; Lund, C. J.; Porter, G. J.; Clarke, R. M.; Zheng, S.-L.; Cundari, T. R.; Betley, T. A. Enantioselective C-H Amination Catalyzed by Nickel Iminyl Complexes Supported by Anionic Bisoxazoline (BOX) Ligands. *J. Am. Chem. Soc.* **2021**, *143*, 817.
(40) Baek, Y.; Das, A.; Zheng, S.-L.; Reibenspies, J. H.; Powers, D. C.; Betley, T. A. C-H Amination Mediated by Cobalt Organoazide Adducts and the Corresponding Cobalt Nitrenoid Intermediates. *J. Am. Chem. Soc.* **2020**, *142*, 11232.
(41) Dong, Y.; Lukens, J. T.; Clarke, R. M.; Zheng, S.-L.; Lancaster, K. M.; Betley, T. A. Synthesis, characterization and C-H amination reactivity of nickel iminyl complexes. *Chem. Sci.* **2020**, *11*, 1260.
(42) Baek, Y.; Betley, T. A. Catalytic C-H Amination Mediated by Dipyrrin Cobalt Imidos. *J. Am. Chem. Soc.* **2019**, *141*, 7797.
(43) King, E. R.; Hennessy, E. T.; Betley, T. A. Catalytic C-H Bond Amination from High-Spin Iron Imido Complexes. *J. Am. Chem. Soc.* **2011**, *133*, 4917.
(44) Hennessy, E. T.; Betley, T. A. Complex N-Heterocycle Synthesis via Iron-Catalyzed, Direct C-H Bond Amination. *Science* **2013**, *340*, 591.
(45) Hennessy, E. T.; Liu, R. Y.; Iovan, D. A.; Duncan, R. A.; Betley, T. A. Iron-mediated intermolecular N-group transfer chemistry with olefinic substrates. *Chem. Sci.* **2014**, *5*, 1526.
(46) Wilding, M. J. T.; Iovan, D. A.; Betley, T. A. High-Spin Iron Imido Complexes Competent for C-H Bond Amination. *J. Am. Chem. Soc.* **2017**, *139*, 12043.
(47) Wilding, M. J. T.; Iovan, D. A.; Wrobel, A. T.; Lukens, J. T.; MacMillan, S. N.; Lancaster, K. M.; Betley, T. A. Direct Comparison of C-H Bond Amination Efficacy through Manipulation of Nitrogen-Valence Centered Redox: Imido versus Iminyl. *J. Am. Chem. Soc.* **2017**, *139*, 14757.
(48) Iovan, D. A.; Wilding, M. J. T.; Baek, Y.; Hennessy, E. T.; Betley, T. A. Diastereoselective C-H Bond Amination for Disubstituted Pyrrolidines. *Angew. Chem., Int. Ed.* **2017**, *56*, 15599.
(49) Davies, H. M. L.; Liao, K. Dirhodium tetracarboxylates as catalysts for selective intermolecular C-H functionalization. *Nat. Rev. Chem.* **2019**, *3*, 347.
(50) Liao, K.; Pickel, T. C.; Boyarskikh, V.; Bacsa, J.; Musaev, D. G.; Davies, H. M. L. Site-selective and stereoselective functionalization of non-activated tertiary C-H bonds. *Nature* **2017**, *551*, 609.
(51) Perera, I. R.; Daeneke, T.; Makuta, S.; Yu, Z.; Tachibana, Y.; Mishra, A.; Bäuerle, P.; Ohlin, C. A.; Bach, U.; Spiccia, L. Application of the Tris(acetylacetonato)iron(III)/(II) Redox Couple in p-Type Dye-Sensitized Solar Cells. *Angew. Chem., Int. Ed.* **2015**, *54*, 3758.
(52) Taber, D. F.; Ruckle, R. E. Cyclopentane construction by dirhodium tetraacetate-mediated intramolecular C-H insertion: steric and electronic effects. *J. Am. Chem. Soc.* **1986**, *108*, 7686.
(53) Clark, J. S.; Dossetter, A. G.; Russell, C. A.; Whittingham, W. G. Anomalous Products from Intramolecular Insertion Reactions of Rhodium Carbenoids into the α-C-H Bonds of Ethers. *J. Org. Chem.* **1997**, *62*, 4910.

https://doi.org/10.1021/jacs.1c02074
J. Am. Chem. Soc. 2021, 143, 7480−7489

(54) Clark, J. S.; Wong, Y.-S.; Townsend, R. J. Probing the mechanism of the anomalous intramolecular C-H insertion reaction of rhodium carbenoids by analysis of kinetic isotope effects. *Tetrahedron Lett.* **2001**, *42*, 6187.
(55) Erhunmwunse, M. O.; Steel, P. G. A novel rearrangement reaction of β-diazo-α-ketoacetals. *Tetrahedron Lett.* **2009**, *50*, 3568.
(56) Tortoreto, C.; Achard, T.; Zeghida, W.; Austeri, M.; Guénée, L.; Lacour, J. Enol Acetal Synthesis through Carbenoid C-H Insertion into Tetrahydrofuran Catalyzed by CpRu Complexes. *Angew. Chem., Int. Ed.* **2012**, *51*, 5847.
(57) Gu, X.; Zhang, Y.; Xu, Z.-J.; Che, C.-M. Iron(III)-salan complexes catalysed highly enantioselective fluorination and hydroxylation of β-keto esters and N-Boc oxindoles. *Chem. Commun.* **2014**, *50*, 7870.
(58) Huang, G.; Ke, M.; Tao, Y.; Chen, F. Specific *Z*-Selectivity in the Oxidative Isomerization of Allyl Ethers to Generate Geometrically Defined Z-Enol Ethers Using a Cobalt(II)(salen) Complex Catalyst. *J. Org. Chem.* **2020**, *85*, 5321.
(59) Neese, F. The ORCA program system. *Wiley Interdiscip. Rev.: Comput. Mol. Sci.* **2012**, *2*, 73.
(60) Hansch, C.; Leo, A.; Taft, R. W. A survey of Hammett substituent constants and resonance and field parameters. *Chem. Rev.* **1991**, *91*, 165.
(61) Sauvé, G.; Deslongchamps, P. Synthesis of *E* and *Z* Alkyl Tetrahydro-2-Pyrilidene and Tetrahydro-2-Furylidene Acetates. *Synth. Commun.* **1985**, *15*, 201.
(62) Anslyn, E. V.; Dougherty, D. A. *Modern Physical Organic Chemistry*; University Science Books: 2006; pp 478−479.
(63) Maldonado-Domínguez, M.; Bím, D.; Fučík, R.; Čurík, R.; Srnec, M. Reactive mode composition factor analysis of transition states: the case of coupled electron-proton transfers. *Phys. Chem. Chem. Phys.* **2019**, *21*, 24912.
(64) Cukier, R. I.; Nocera, D. G. Proton-Coupled electron transfer. *Annu. Rev. Phys. Chem.* **1998**, *49*, 337.
(65) Cheng, R.; Wu, C.; Cao, Z.; Wang, B. QM/MM MD simulations reveal an asynchronous PCET mechanism for nitrite reduction by copper nitrite reductase. *Phys. Chem. Chem. Phys.* **2020**, *22*, 20922.
(66) Jeong, Y. J.; Kang, Y.; Han, A.-R.; Lee, Y.-M.; Kotani, H.; Fukuzumi, S.; Nam, W. Hydrogen Atom Abstraction and Hydride Transfer Reactions by Iron(IV)-Oxo Porphyrins. *Angew. Chem., Int. Ed.* **2008**, *47*, 7321.
(67) Becke, A. D. Density-functional exchange-energy approximation with correct asymptotic behavior. *Phys. Rev. A: At., Mol., Opt. Phys.* **1988**, *38*, 3098.
(68) Perdew, J. P. Density-functional approximation for the correlation energy of the inhomogeneous electron gas. *Phys. Rev. B: Condens. Matter Mater. Phys.* **1986**, *33*, 8822.
(69) Schäfer, A.; Horn, H.; Ahlrichs, R. Fully optimized contracted Gaussian basis sets for atoms Li to Kr. *J. Chem. Phys.* **1992**, *97*, 2571.
(70) Schäfer, A.; Huber, C.; Ahlrichs, R. Fully optimized contracted Gaussian basis sets of triple zeta valence quality for atoms Li to Kr. *J. Chem. Phys.* **1994**, *100*, 5829.
(71) Shannon, R. Revised effective ionic radii and systematic studies of interatomic distances in halides and chalcogenides. *Acta Crystallogr., Sect. A: Cryst. Phys., Diffr., Theor. Gen. Crystallogr.* **1976**, *32*, 751.
(72) Robert, J. D.; Caserio, M. C. *Basic Principles of Organic Chemistry*, 2nd ed.; W. A. Benjamin: 1977; pp 1287−1341.
(73) Anslyn, E. V.; Dougherty, D. A. *Modern Physical Organic Chemistry*; University Science Books: 2006; pp 478−479.
(74) Anslyn, E. V.; Dougherty, D. A. *Modern Physical Organic Chemistry*; University Science Books: 2006; pp 35−51.
(75) Luo, Y. R. *Comprehensive Handbook of Chemical Bond Energies*; CRC Press: Boca Raton, FL, 2007; pp 19−147.
(76) Vitaku, E.; Smith, D. T.; Njardarson, J. T. Analysis of the Structural Diversity, Substitution Patterns, and Frequency of Nitrogen Heterocycles among U.S. FDA Approved Pharmaceuticals. *J. Med. Chem.* **2014**, *57*, 10257.
(77) Anslyn, E. V.; Dougherty, D. A. *Modern Physical Organic Chemistry*; University Science Books: 2006; pp 4−26.
(78) Perron, F.; Albizati, K. F. Chemistry of spiroketals. *Chem. Rev.* **1989**, *89*, 1617.

https://doi.org/10.1021/jacs.1c02074
J. Am. Chem. Soc. 2021, 143, 7480−7489